The Pennsylvania State University

The Graduate School

Department of Engineering Science and Mechanics

EXPLORING NANOSTRUCTURES FOR APPLICATIONS IN HUMIDITY SENSING AND ACTIVE PLASMONICS

A Thesis in

Engineering Science

by

Thomas R. Walker

Submitted in Partial Fulfillment
of the Requirements
for the Degree of

Master of Science

December 2008

The thesis of Thomas R. Walker was reviewed and approved* by the following:

Tony Jun Huang
James Henderson Assistant Professor of Engineering Science and Mechanics
Thesis Advisor

Jian Xu
Assistant Professor of Engineering Science and Mechanics

Sulin Zhang
Assistant Professor of Engineering Science and Mechanics

Judith A. Todd
Head of the Department of Engineering Science and Mechanics
Professor of Engineering Science and Mechanics

*Signatures are on file in the Graduate School

ABSTRACT

An optical humidity sensor based on a nanoporous, polymeric photonic crystal (PC) is demonstrated. The PC sensing structure is created by combining a holographic interference patterning technique with a modified holographic, polymer-dispersed liquid crystal system. Changes in relative humidity (RH) induce the modification of the refractive index contrast between the nanoporous and nonporous regions — and thus between the transmittance and bandgap position — of the PC structure. For a PC structure with 30% porosity and a grating spacing of 220 nm, a change in the RH from 40% to 95% at 34°C results in a redshift of 43 nm in the central wavelength at the PC bandgap and an increase from 12% to 87% in the relative transmittance at λ = 600 nm. Other performance analyses have shown that the nanoporous polymeric PC-based humidity sensor is highly stable and reproducible, exhibits minimal hysteresis, and responds relatively fast.

Further, we have fabricated close-packed arrays of gold-coated polystyrene nanospheres upon PDMS substrates. By stretching and squeezing the PDMS, we controllably, reversibly changed the plasmonic properties of the arrays. We also simulated by a finite-difference time-domain method how rearranging such arrays affects their plasmonic properties.

TABLE OF CONTENTS

LIST OF FIGURES

ACKNOWLEDGEMENTS

The author thanks Yue Bing Zheng, Jinjie Shi, and Xiaole Mao for essential discussion.

Chapter 1

Humidity Sensing

Humidity control and monitoring have increasingly attracted attention in recent decades due to their importance in agriculture, environment, medicine, and the semiconductor industry [1–5]. Thus far, most studies on humidity-sensing materials have focused on porous ceramics [6–12] and polymers [13–20]. Porous polymers and ceramics have large surface-to-volume ratios, which allow highly sensitive detection of surface alterations that are caused by the adsorption/desorption of water vapor. In recent years, an increasing number of studies on porous polymer-based humidity sensors have been reported, due to polymers' advantages such as low cost, ease of processing, high sensitivity, and excellent mechanical and chemical stability. Changes in the resistance, capacitance, or optical properties of porous polymers under different relative humidity (RH) can serve as humidity-sensing mechanisms [21–25].

We report the design, fabrication, and characterization of nanoporous, polymeric, one-dimensional photonic crystals (PC) as a platform for optical humidity sensing. Compared with resistance-based or capacitance-based humidity sensors, optical sensors are immune to electrical noise and have high detection sensitivity. The PCs are created by combining a holographic interference patterning technique with a modified holographic, polymer-dispersed liquid crystal (H-PDLC) system [26,27]. Humidity sensing is achieved through two mechanisms: changes in the RH-dependent refractive index (RI) contrast between the nanoporous and nonporous regions, and reversible swelling of the polymeric structure at high RH regions. Both mechanisms change the transmission intensity and the bandgap position of the PC structures. The described humidity sensors feature a convenient fabrication process, amenability for miniaturization, high detection

sensitivity, excellent stability and reproducibility over a wide range of RH, fast response time, and only slight hysteresis.

Experiment

Sample Fabrication

Nanoporous, polymeric, one-dimensional PC structures were fabricated per a holographic photopolymerization process [28–30]. The fabrication setup is shown in Fig. 1-1. A homogeneous prepolymer syrup was formed by thoroughly mixing a monomer (60 wt.% dipentaerythritol hydroxypentaacrylate from Aldrich), a photo-initiator (1 wt.% Rose Bengal from Spectra Group Limited), a co-initiator (3 wt.% N-phenylglycine from Aldrich), liquid crystals (15 wt.% TL213 from Merck), non-reactive solvent (15 wt.% toluene from Aldrich), and 3-Aminopropyltriethoxysilane (APTES, 6 wt.% from Aldrich). The syrup was then sandwiched between two pieces of glass. The distance between the two glass slides was precisely controlled by adding microbeads (3 μm diameter) at the edge of the syrup, thereby defining the thickness of the PC structure. A 100 mW argon ion laser (λ= 514 nm, 10% P-polarized and 90% S-polarized) was used to generate an incident beam. In order to achieve a better interference pattern, the incident laser beam was split by an S-polarized beam splitter to remove the P-polarized component. After being altered and collimated, the laser beam was guided to pass into a prism. Thus, the incident beam and its total internal reaction created an interference pattern in the syrup. A one-dimensional PC was fabricated by periodic modulation of the high and low optical intensities in the interference pattern. The modulation period of the polymeric PC was controlled by tuning the incident angle of the collimated beam. After being exposed to the interference patterning for 30 s, the samples were post-cured for 24 h in a chemical fume hood. Upon

separating the sample from the cover slide, a nanoporous, polymeric PC structure situated on a glass slide was obtained (schematic is shown in the inset of Fig. 1-1).

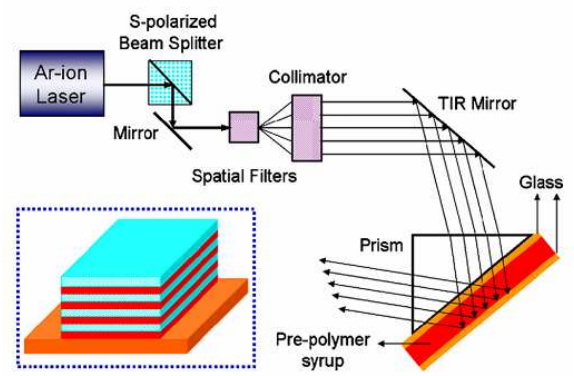

Figure **1-1**: Schematic of the experimental setup for the fabrication of a nanoporous, polymeric, one-dimensional PC. Optical components including an argon ion laser, a beam splitter, spatial filters and collimators were precisely positioned on an optical table. A holographic interference pattern formed on the pre-polymer syrup sandwiched between two glass slides. The inset is a schematic of a one-dimensional PC situated on a glass substrate.

Figs. 1-2(a) and (b) show the cross-sectional morphology of a nanoporous, polymeric PC sample as observed by bright field trans- mission electron microscopy (BF-TEM) and scanning electron microscopy (SEM), respectively. One of the nanoporous regions is enclosed by a dashed square in both the SEM and the TEM images. The pore diameters range from a few nanometers to tens of nanometers, and the porosity of the polymeric PC structure is roughly 30%.

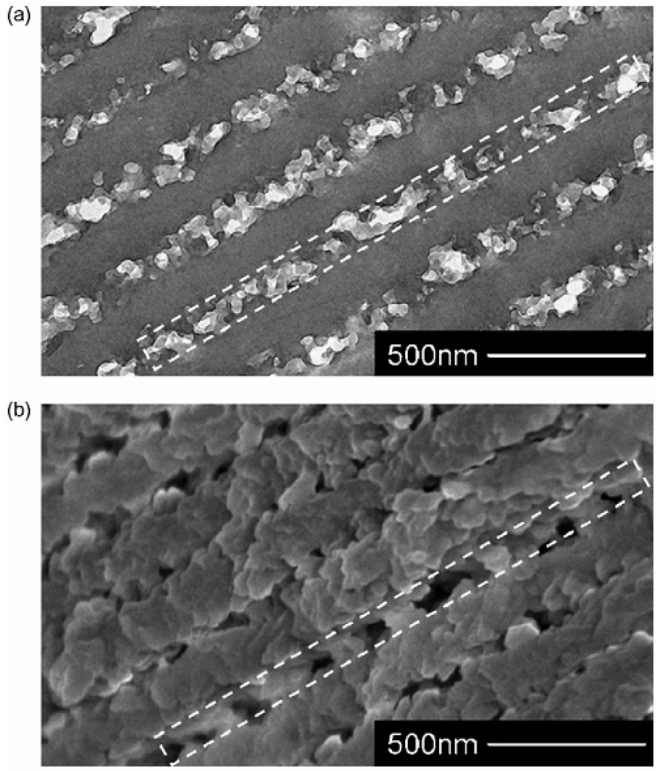

Figure **1-2**: (a) TEM and (b) SEM images of the cross-sectional morphology of a nanoporous, polymeric, one-dimensional PC. The grating spacing of the PC is about 220 nm. Dashed rectangles are used in both (a) and (b) to enclose one of the nanoporous regions.

Measurement Principle

The bandgap characteristic of a PC is determined by its RI contrast and filling ratio [31,32]. For the nanoporous, polymeric PC structure used in this work, the RI contrast between the nanoporous and nonporous regions plays a key role in its bandgap behavior. With increasing RH, the nanoporous regions adsorb water molecules and the RI of these regions increases. Meanwhile, the nonporous regions barely adsorb water molecules and the RI remains constant. As a result, the RI contrast between the nanoporous and nonporous regions decreases, the bandgap position redshifts, and the transmittance at the bandgap increases. In addition, at high

RH regions, minor reversible swelling of the polymeric PC structure occurs, causing changes in the filling ratio, the bandgap position, and the transmittance. Thus, the humidity sensing of our nanoporous polymeric PC structures is based on two mechanisms: changes in the RH-dependent RI contrast between the nanoporous and nonporous regions, and reversible swelling of the polymeric structure at high RH regions.

Measurement Setup

Fig. 1-3 depicts the schematic of the optical measurement setup for humidity sensing. White light produced by a halogen lamp (LS-1 Tungsten Halogen Light Source, Ocean Optics Co.) was used as the source beam in the experiments. Two optical fibers were aligned on both sides of a glass/PC sample using fiber holders. The fibers were fixed in the fiber holders using connectors (SMA 905, Ocean Optics Co.) with integrated collimating lenses (200–2000 nm 74-UV collimating lens, Ocean Optics Co.). The PC sample coated on a glass substrate was fixed on a Teflon base to ensure that the PC structure was normal to the collimated light (with divergent angle less than 2°). After passing through the sample, the light was collected, collimated, and guided to a spectrometer (HR4000, Ocean Optics Co.) where the transmitted optical signal was measured for a spectral range of 400–1000 nm. A humidity chamber (ESPEC North America Inc., SH-241) was used to control the operating temperature and humidity. The RH inside the humidity chamber could be adjusted to any number between 40% and 95%. However, since the chamber required almost 15 min to adjust humidity, a smaller quartz chamber (4 cm x 4 cm x 4 cm) and an oscillating water vapor source (between 20% and 100% RH) were used to characterize the response time.

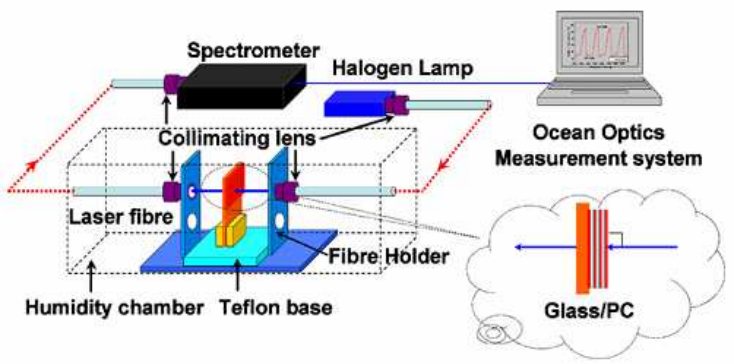

Figure **1-3**: Schematic of the humidity-sensing measurement setup. The polymeric PC structure coated on a glass substrate was fixed upon a Teflon base, and two optical fibers (source and readout) were aligned by fibre holders and located within a humidity chamber. A halogen lamp was used to generate white incident light. Output signals were analyzed and recorded with a software-controlled spectrometer.

Results and Discussion

Fig. 1-4(a) shows the spectral response of the nanoporous polymeric PC to different RHs at a constant temperature (34°C). The central wavelength Δ_{Bragg} of the photonic bandgap for the polymeric PC structure redshifted from 615 to 658 nm as the RH was increased from 40% to 95%. Δ_{Bragg} can be estimated using Bragg's law [33]:

$$\Delta_{Bragg} = 2\, n_{ave}\, \Lambda$$

where n_{ave} is the average refractive index and Λ is the grating spacing. At 40% RH, n_{ave} is estimated as 1.404, assuming 30% porosity, $n_{polymer} = 1.52$, $n_{air} = 1$, and $n_{water} = 1.33$. Based on Eq. (1) and the data presented in Fig. 1, the grating spacing Λ was calculated to be 219 nm, which is in excellent agreement with the TEM/SEM measurement results (roughly 220 nm) from Fig. 1-2. When the RH was changed to 95%, n_{ave} was measured to be 1.459, and the grating spacing is calculated to be 225 nm, which indicates that minor swelling of the polymeric structure occurs at a high-humidity environment. In order to test the long-term stability of this polymeric PC structure at high RH, the spectra at 95% RH were recorded continuously for 4 h (Fig. 1-4(b)). The

central wavelength and transmittance of the bandgap remained unchanged during this time period, indicating the sensor's excellent stability at high RH regions.

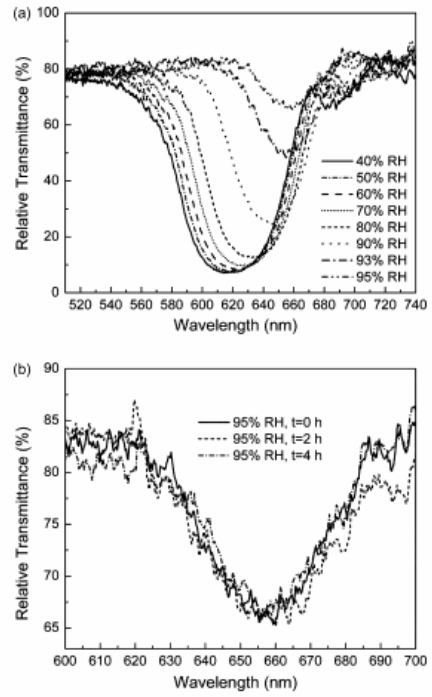

Figure **1-4**: (a) The transmittance spectra of a typical nanoporous polymeric PC at various RH. (b) The transmittance spectra of the PC at 95% RH recorded at t = 0, 2 and 4 h. The relative transmittance is the ratio of the transmitted signal to the normalized incident light.

Fig. 1-4(a) also shows that the transmittance at the PC bandgap increases with RH. This phenomenon is caused by the variations in the RI contrast between the nanoporous and nonporous regions and the minor swelling of the polymeric PC structure at high-RI regions. Higher humidity will lead to lower RI contrast and thus higher transmittance at the PC bandgap. As water vapor saturates the nanopores, the PC structure becomes more isotropic (the RI of water vapor is closer to that of the polymer than to that of the air voids) and its bandgap effect diminishes, resulting in increasing transmitted intensity at the bandgap. The increase of relative transmittance with RH suggests that the structure can be used as a quantitative humidity sensor. Moreover, the total

transparency of the polymeric PC structure also changes as the bandgap redshifts; this mechanism makes the structure suitable as a portable colorimetric humidity sensor.

Fig. 1-5 depicts the dependence of transmittance on RH at several characteristic wavelengths. When the chosen characteristic wavelength decreases from 615 nm (the central bandgap wavelength at 40% RH) to 565 nm, the magnitude of change in relative transmittance decreases and the relative transmittance-versus-RH curves exhibit greater linearity. These results suggest that our humidity sensors offer tunable sensitivity and linearity.

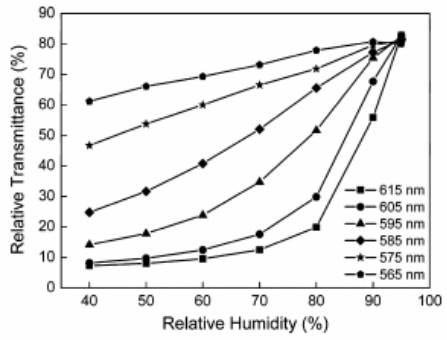

Figure **1-5**: The dependence of relative transmittance on RH at different characteristic wavelengths.

Fig. 1-6 shows the variation of relative transmittance (λ = 600 nm) to an RH-increasing and -decreasing cycle. When RH is changed from 40% to 95%, the relative transmittance increases from 12% to 87%, indicating high sensitivity. Here we define the detection sensitivity as the ratio of the change in relative transmittance to the RH change ($\Delta I/\Delta RH$) at a certain wavelength in the bandgap. The sensor also demonstrates excellent stability and reversibility because its transmittance returns to the same value after one humidity increasing/decreasing cycle.

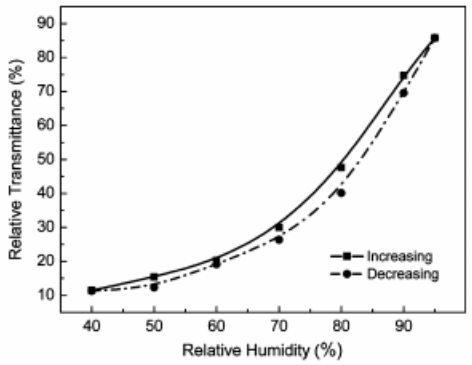

Figure **1-6**: Variation of the relative transmittance at 600 nm to an RH increasing/decreasing cycle. The solid squares represent the adsorption (RH increasing) process, and the circles represent the desorption (RH decreasing) process.

Minor hysteresis is observed during the cycle. It is likely due to the different mass transport kinetics between the vapor adsorption and desorption processes. The difference in mass transport kinetics results in unequal amounts of water molecules trapped in the nanopores for the two processes (adsorption and desorption) at the same RH. The hysteresis observed in our system is considered minor compared to the results from previously reported studies [22,34].

The stability and repeatability of the humidity sensors over a large RH range is further demonstrated in a multi-cycle experiment in which saturated water vapor (100% RH) was periodically introduced to the smaller quartz humidity chamber where the RH was maintained to be 20%. Fig. 1-7 shows that as the RH periodically oscillates between 20% and 100%, the relative transmittance at the wavelength of 595 nm switches between 15% and 98%. This response is highly reproducible as we see that the difference in relative transmittance for more than 100 experimental cycles is less than 1%. Fig. 1-7 also shows that the humidity sensor responds more quickly to the adsorption process (from 20% to 100% RH) than to desorption (from 100% to 20% RH). This indicates that it takes longer for water molecules to diffuse from nanopores to the environment than by the opposite route. It is observed that the relative transmittance changes from 15% (almost opaque) at 20% RH to 98% (transparent) at 100% RH.

This large change in transmittance enables convenient, sensitive, and cost-efficient optical measurement using a single wavelength (595 nm).

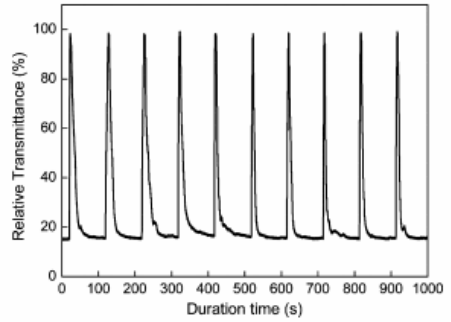

Figure **1-7**: The time-dependent transmittance curve (λ = 595 nm, T =20°C) as the RH oscillates between 20% and 100% for multiple cycles.

Fig. 1-8 indicates that the response time for the adsorption process (from 20% to 100% RH) is about 1.5 s, while Fig. 1-7 shows that the desorption process takes 20–30 s. The response time and sensitivity of the sensor are dependent upon its porosity. Based on Eq. (1), the bandgap position of a PC structure is dependent upon its average RI. Higher porosity or smaller pore size leads to a larger surface-to-volume ratio; more water molecules are trapped in the nanopores. As a result, the change in the average RI is larger, and the shift of the bandgap position is more significant. By adjusting the porosity, film thickness and grating spacing, one may realize nanoporous, polymeric, PC-based humidity sensors that can meet different requirements in response time and bandgap shift.

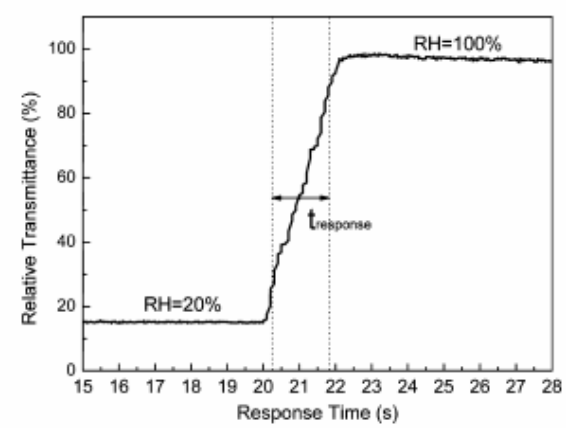

Figure **1-8**: The time-dependent transmittance curve (λ = 595 nm, T =20°C) as the RH increases from 20% to 100%.

Conclusion

A humidity sensor based on a nanoporous polymeric PC structure is shown to be sensitive, robust, quickly responding, and cost efficient. The PC sensing structure is fabricated by combining a holographic interference patterning technique with a modified H-PDLC system. The bandgap of the PC structure shifts when water vapor penetrates the nanopores, changing the RI contrast between the porous and nonporous regions. For a PC structure with 30% porosity and a grating spacing of 220 nm, as the RH changes from 40% to 95% at 34°C, the central wavelength of the PC bandgap redshifts 43 nm and the relative transmittance at λ = 600 nm increases from 12% to 87%. The nanoporous, polymeric, PC-based humidity sensor demonstrates excellent reversibility and reproducibility. When the RH oscillates between 20% and 100%, the relative transmittance at 595 nm reproducibly switches between 15% and 98%. Less than 1% difference in the relative transmittance upon the same RH (20% or 100%) is observe7d upon hundreds of experimental cycles. The response time for the absorption process is about 1.5 s, and the

desorption process takes 20–30 s. Moreover, the response time and the bandgap shift can be optimized by altering fabrication parameters such as porosity and grating spacing [35].

References

1 Chen, Z. and C. Lu, *Humidity sensors: a review of materials and mechanisms*, Sens. Lett., 2005. **3**: p. 274–295.

2 Arai, H. and T. Seiyama, in: W. Göpel (Ed.), *Sensors: A Comprehensive Survey*, 3, VCH, Weinheim, Germany, 1992, p. 981–1012.

3 Fenner, R. and E. Zdankiewicz, *Micro-machined water vapor sensors: a review of sensing technologies*, IEEE Sens. 14, 2001. **14:** p. 309–317.

4 Huang, J.R. et al., *A novel conductive humidity sensor based on field ionization from carbon nanotubes*, Sens. Actuators A, 2007. **133**: p. 467–471.

5 Yamazoe, N. and Y. Shimizu, *Humidity sensors: principles and applications*, Sens. Actuators, 1986. **10**: p. 379–398.

6 Kulwicki, B.M., *Humidity sensors*, J. Am. Ceram. Soc., 1991. **74**: p. 697–708.

7 Kang, U. and K.D.Wise, *A high-speed capacitive humidity sensorwith on-chip thermal reset*, IEEE Trans. Electron. Devices, 2000. **47**: p. 702–710.

8 Seiyama, T., N. Yamazoe and H. Arai, *Ceramic humidity sensors*, Sens. Actuators, 1983. **4**: p. 85–96.

9 Traversa, E., *Ceramic sensors for humidity detection: the state-of-the-art and future developments*, Sens. Actuators B, 1995. **23**: p. 135–156.

10 Kalkan, A.K. et al., *A rapid-response, high-sensitivity nanophase humidity sensor for respiratory monitoring*, IEEE Electron. Device Lett., 2004. **25**: p. 526–528.

11 Connolly, E.J. et al., , *Relative humidity sensors using porous SiC membranes and Al electrodes*, Sens. Actuators B, 2004. **100**: p. 216–220.

12 Zambov, L.M. et al., *Capacitance humidity sensor with carbon nitride detecting element*, Appl. Phys. A, 2000. **70**: p. 603–606.

13 Tsigara, A., *Hybrid polymer/cobalt chloride humidity sensors based on optical diffraction*, Sens. Actuators B, 2007. **120**: p. 481–486.

14 Wang, J. et al., *Study of polymer humidity sensor array on silicon wafer*, J. Mater. Sci., 2004. **39**: p. 3155–3157.

15 Zajt, T., G. Jasinski and B. Chachuiski, *Electrical properties of polymer humidity sensor based on polyethyleneimine*, Proc. SPIE, 2003. **5124**: p. 130–137.

16 Rubinger, C.P.L. et al., *Sulfonated polystyrene polymer humidity sensor: synthesis and characterization*, Sens. Actuators B, 2007. **123**: p. 42–49.

17 Nomura, T. et al., *Humidity sensor using surface acoustic waves propagating along polymer/LiNbO3 structures*, Ultrason. Symp., 1993. p. 417–420.

18 Nomura, T. et al., , *SAW humidity sensor using dielectric hygroscopic polymer film*, Ultrason. Symp., 1994. p. 503–506.

19 Sakai, Y. et al., *A humidity sensor composed of interpenetrating polymer networks of hydrophilic and hydrophobic methacrylate polymers*, J. Electrochem. Soc., 1993. **140**: p. 432–436.

20 Wang, J. et al., *Humidity sensitivity of composite material of lanthanum ferrite/polymer quaternary acrylic resin*, Sens. Actuators B, 2004. **99**: p. 586–591.

21 Zanjanchi, M.A. and Sh. Sohrabnezhad, *Evaluation of methylene blue incorporated in zeolite for construction of an optical humidity sensor*, Sens. Actuators B, 2005. **105**: p. 502–507.

22 Steele, J.J. et al., , *Nanostructured gradient index optical filter for high-speed humidity sensing*, Sens. Actuators B, 2006. **120**: p. 213–219.

23 Yang, B. et al., *Compliant and low-cost humidity sensors using nano-porous polymer membranes*, Sens. Actuators B, 2006. **114**: p. 254–262.

24 Albrecht, B.A. et al., *Polymer capacitance sensors for measuring soil gas humidity in drier soils*, Geotech. Test. J., 2003. **26**: p. 3–11.

25 Yao, Z. and M. Yang, *A fast response resistance-type humidity sensor based on organic silicon containing cross-linked copolymer*, Sens. Actuators B, 2006. **117**: p. 93–98.

26 Matsuoka, S., V.T. Wallder and H.L. Beauchamp, *Application of holographic interference technique to mechanical studies of polymeric solids*, Polym. Eng. Sci., 1971. **11**: p. 46–50.

27 Bunning, T.J. et al., *Holographic polymer-dispersed liquid crystals (H-PDLCS)*, Annu. Rev. Mater. Sci., 2000. **30**: p. 83–115.

28 Hsiao, V.K.S. et al., *Optical microfabrication of highly reflective volume Bragg gratings*, Appl. Phys. Lett., 2005. **86**: p. 131113.

29 Natarajan, L.V., *Switchable holographic polymer-dispersed liquid crystal reflection gratings based on thiol-end photopolymerization*, Chem. Mater., 2003. **15**: p. 2477–2484.

30 Hsiao, V.K.S., *Organic solvent vapor detection using holographic photopolymer reflection gratings*, Adv. Mater., 2005. **17**: p. 2211–2214.

31 Yablonovitch, E. and T.J. Gmitter, *Photonic band structure: the face-centered-cubic case*, Phys. Rev. Lett., 1989. **63**: p. 1950–1953.

32 Berger, V., *From photonic band gaps to refractive index engineering*, Opt. Mater., 1999. **11**: p. 131–142.

33 Kogelnik, H., *Coupled wave theory for thick hologram gratings*, Bell Syst. Tech. J., 1969. **48**: p. 2909–2947.

34 Madamopoulos, N. et al., *Polymer based photonic sensors for physicochemical monitoring*, Proc. SPIE, 2005. **5993**: p. 599308.

35 Shi, J. et al., *Humidity sensing based on nanoporous polymeric photonic crystals*, Sens. Act. B, 2008. **129**: p. 391–396.

Chapter 2

Active Plasmonics

Plasmonics concerns the fluctuation of electrons near the surfaces of noble metals. When these "surface plasmons" interact with photons that are incident upon the surface, a result is the near-field localization of light. This localization is altered by the presence of any substance which contacts the metal.[1-4] As such, surface plasmons are exploited in nanophotonic devices[5-9] and biomedical applications.[10-13]

These exploitations demand especial sensitivity to changes in the localization of light. Many of them measure changes in localized surface plasmon resonance (LSPR), which is specific to noble metal nanostructures.[14, 15] Some advantages of using LSPR as a sensing mechanism include selectivity[16] and sensitivity[17] that are tunable with the size of the metal particles, as well as real-time measurement.[18] LSPR is plotted as typically plotted as absorption of light over a spectrum of wavelengths. The absorption plot of an array of noble metal nanostructures will exhibit one or more peaks. These peaks are sensitive to the geometries of the nanostructures, the environment surrounding them, and *the spacing between them*.[19-23] Such sensitivities have spurned researchers to fabricate noble metal nanostructures of many different shapes (*e.g.*, toruses, cubes, rods, and shells).[24-27]

One *might* fabricate noble metal nanostructures of a specific geometry or in a specific medium in order to realize LSPR peaks at desired wavelength. A more-flexible approach is to actively tune the LSPR peak after fabricating the nanostructures. Such an approach was termed a*ctive plasmonics* (AP) by Krasavin and Zheludev, who exploited the thermal expansion of Ga to achieve all-optical, mW-power switching of metallic monolayers.[28] Applications of active

plasmonics include optical gates, photodetectors, nanophotonic circuits, molecular imaging, metamaterials, and optical memory elements.[1, 29] One might also control Raman scattering, a phenomenon that is characteristic of a material's density of states and resonant modes.[16, 30-36]

Applications of active plasmonics require the low-cost fabrication of noble metal nanostructures or films that are upon or within a resilient medium. When the medium is manipulated, the metal must exhibit a significant LSPR shift (more than a few nm).[1, 15, 28, 37] Previous work in this vein is lacking:

- Malynych and Chumanov in 2003 fabricated unordered silver nanoparticles on a flexible substrate that when stretched exhibited a *marginal* LSPR shift.[38]
- Herrmann *et al*. in 2007 developed a strain gauge of gold nanoparticles patterned in an array upon a polymeric substrate. A voltage was applied to the unstretched array. When the substrate was stretched, the uniaxial separation of gold nanoparticles resulted in a change in voltage. This change served as a mechanism to detect strain.[39] *The optical properties of this setup were not investigated, however.*
- Tao *et al.* in 2007 fabricated films of silver nanoparticles by the Langmuir-Blodgett technique, and then measured the plasmonic properties of various arrangements of the films.[40] However, such arrangements are not tunable after fabrication, so the method is *passive.*

We fabricated close-packed arrays of gold-coated polystyrene nanospheres upon PDMS substrates. (Yan *et al.* in 2005 similarly patterned arrays of nanospheres on flexible substrates; when stretched, the substrates rearranged the nanostructures from hexagonal arrangments to rows.[41]) By stretching and squeezing the PDMS, we controllably and reversibly changed the

plasmonic properties of the arrays. We also simulated by a finite-difference time-domain method how rearranging such arrays affects their plasmonic properties.

Experiment

Sample Fabrication

Polystyrene (PS) nanospheres were obtained in-solution (10 wt%; Bangs Laboratories). Two solutions containing PS of nominal mean diameters ~0.80 μm and ~1.05 μm were used in separate experiments.

Smooth PDMS was fabricated as a substrate onto which the PS nanospheres were later deposited. To ensure the smoothness of the PDMS surfaces, the PDMS was cast againt silicon wafers (which are extremely flat). The wafers were first cleaned by acetone, isopropanol (IPA) and deionized (DI) water. PDMS was mixed upon the surface and cured at 70°C for one hour.

A KSV Minitrough (KSV Instruments) was used to compress the monolayers of PS nanospheres. The trough was cleaned with IPA and DI water; each liquid was suctioned out with a vacuum pump. The trough was filled with DI water. A volume of PS solution on the order of microliters was diluted 1:10 with ethanol. PS nanospheres were deposited on the surface of the DI water, and they were dispersed on the surface upon the addition of several microliters of sodium dodecyl sulfate. The barriers of the trough were compressed to form a close-packed monolayer of PS nanospheres. This monolayer was directly transferred onto the surface of the PDMS by touching the PDMS to the surface of the liquid. The liquid surrounding the transferred

monolayer was allowed to evaporate, leaving only the PS on the PDMS. The PS nanospheres were thereafter sputtered with gold.

Measurement Setup

A spectrometer (Ocean Optics) capable of measuring light in the ultraviolet-visible-infrared (UV-vis-IR) range was used to measure absorption of Au nanostructures upon stretching the underlying substrates. The substrates were affixed to calipers of precision 0.01 mm (Mitotoyo). The movable end of the calipers was fixed between the detectors of the spectrometer. This setup is schematically illustrated in Figure 2-1. For the two distinct sizes of PS, absorption spectra were recorded for various amounts of stretching over absorbance wavelengths ranging from 400 nm to 900 nm. These spectra were plotted in OriginPro 8.0 (OriginLab Corp.).

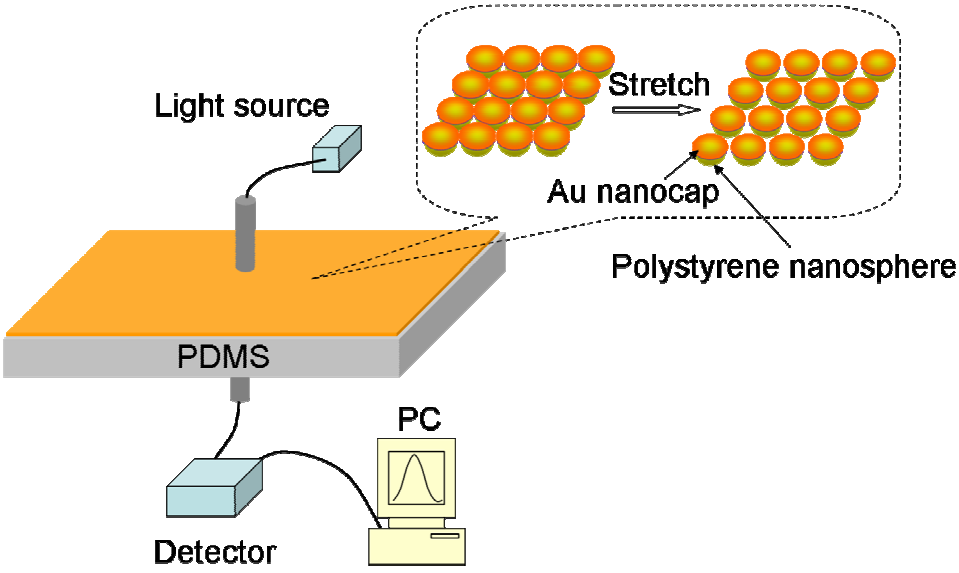

Figure **2-1**: Setup for recording absorption of Au nanostructures while stretching the underlying substrates. Each substrate was affixed to calipers of precision 0.01 mm. For both sizes of Au nanostructures, photospectra were recorded for various amounts of stretching over absorption wavelengths ranging from ~400 nm to ~900 nm.

Results and Discussion

We took images of PS nanospheres by optical microscope (using a 100*x* objective lens) to show that nanostuctures move significantly and predicatibly when the underlying substrate is manipulated. Figure 2-2 shows polystyrene nanospheres of mean diameter 1.05 μm as-deposited on a PDMS substrate. The nanospheres in Figure 2-2a were not subject to stretching; they were close-packed and hexagonally arranged. Figure 2-2b shows the same substrate being stretched 1000 μm; the nanospheres were still close-packed, but they were linearly rearranged. Likewise, Figure 2-2c shows the same substrate being stretched 2000 μm. In all three figures, we defined three rows (1, 2 and 3) of nanoparticles. As follows, we tracked for several locations upon the 1.05 μm sample how the interparticle distances changed with different amounts of stretching

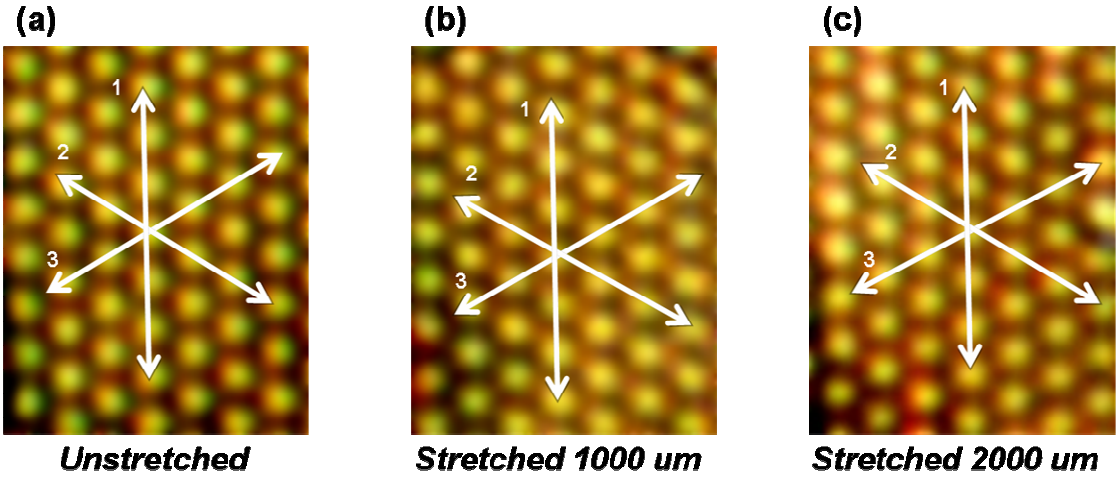

Figure **2-2**: Optical images of PS nanospheres upon a PDMS substrate which was **(a)** unstretched, **(b)** stretched 1000 μm, and **(c)** stretched 2000 μm. The substrates were observed under a 100*x* objective lens.

Figures 2-3a, b and c are plots of interparticle changes in distance along the three different rows respectively labeled Rows 1, 2 and 3, upon stretching of the substrates from 0 to 2000 μm. We averaged each change in distance over several locations upon the substrate. The distances were recorded in arbitrary units. Figure 2-3a (corresponding to Rows 1, those which are vertical) shows a small *decrease* in interparticle distances. In contrast, Figures 2-3b and 2-3c

(respectively corresponding to Rows 2 and 3, those which are slanted) show much-greater *increases* in interparticle distances.

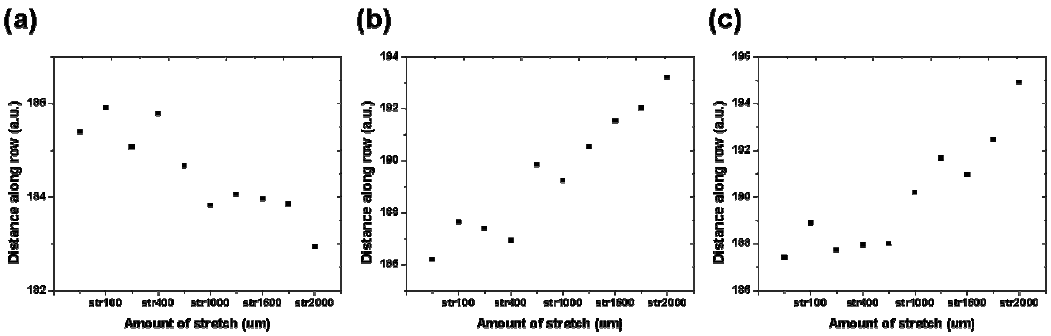

Figure **2-3**: Interparticle changes in distance along **(a)** Rows 1, **(b)** Rows 2 and **(c)** Rows 3, upon stretching of the substrates from 0 to 2000 μm. Each change in distance was averaged over several locations upon the substrate. The distances were recorded in arbitrary units.

Figures 2-4a and 2-4b are absorbance spectra for *stretching* the substrates which supported, respectively, the 0.80 μm and 1.05 μm samples. We plotted the spectra for 200 μm increments of stretching from 0 μm to 2000 μm. Both the 0.80 and 1.05 μm samples exhibited slight redshifts for small amounts of stretch, followed by substantial blueshifts for further stretching. The shifts were repeatable and reversible over several trials and in several locations with the arrays. Figures 4c and 4d are the peak shifts when stretching, respectively, the 0.80 μm and 1.05 μm samples. The solid lines in Figures 2-4c and 2-4d are to guide the eye.

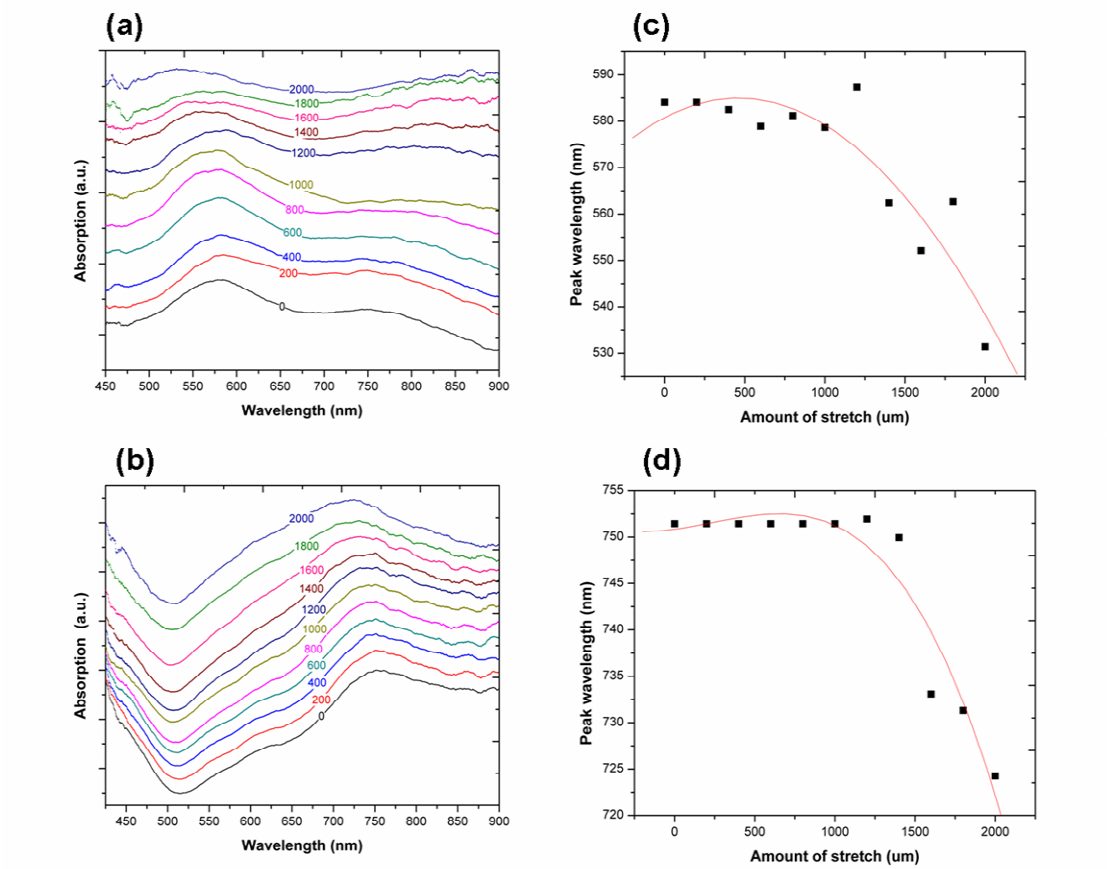

Figure **2-4**: (a) Absorption spectra for the stretched 0.80 μm sample and (b) the stretched 1.05 μm sample. Shifts in the spectra were repeatable and reversible over several trials and in several locations with the arrays. (c) Peak shifts for the 0.80 μm sample and (d) the 1.05 μm sample. The solid lines are to guide the eye.

Conclusion

We fabricated upon flexible substrates several arrays of Au nanostructures which featured long-range order. We investigated the plasmonic properties of said arrays upon stretching the substrate – the arrays exhibited repeatable, reversible LSPR shifts. Further, we confirmed that the nanostructures were consistently separating along each row, to ensure that the LSPR shifts were not due to other geometrical changes. Additional support for this notion is forthcoming by way of theoretical calculations of the LSPR.

References

1. Zheng, Y.B. and T.J. Huang, *Surface plasmons of metal nanostructure arrays: from nanoengineering to active plasmonics.* Journal for the Association of Labratory Automation, 2008. **13**: p. 215-226.
2. Maier, S.A., et al., *Plasmonics - a route to nanoscale optical devices.* Advanced Materials, 2001. **13**: p. 1501-1505.
3. Kreibig, U. and M. Vollmer, *Optical Properties of Metal Clusters*. 1995, Berlin Heidelberg: Springer-Verlag.
4. Raether, H., *Surface plasmons on smooth and rough surfaces and on gratings* in *Springer Tracts in Modern Physics*. 1988, Springer: Berlin.
5. Atwater, H.A., et al., *The new "p–n junction": plasmonics enables photonic access to the nanoworld.* MRS Bulletin, 2005. **30**: p. 385.
6. Barnes, W.L., A. Dereux, and T.W. Ebbesen, *Surface plasmon subwavelength optics.* Nature, 2003. **424**: p. 824-830.

7. Fang, N., et al., *Sub-diffraction-limited optical imaging with a silver superlens.* Science, 2005. **308**: p. 534-537.

8. Ozbay, E., *Plasmonics: merging photonics and electronics at nanoscale dimensions.* Science, 2006. **311**: p. 189-193.

9. Zia, R., et al., *Plasmonics: the next chip-scale technology.* Materials Today, 2006. **9**: p. 20-27.

10. Endo, T., et al., *Multiple label-free detection of antigen-antibody reaction using localized surface plasmon resonance-based core-shell structured nanoparticle layer nanochip.* Analytical Chemistry, 2006. **78**: p. 6465-6475.

11. Haes, A.J., et al., *Detection of a biomarker for Alzheimer's disease from synthetic and clinical samples using a nanoscale optical biosensor.* Journal of the American Chemical Society, 2005. **127**: p. 2264-2271.

12. Loo, C., et al., *Immunotargeted nanoshells for integrated cancer imaging and therapy.* Nano Letters, 2005. **5**: p. 709-711.

13. Rosi, N.L., et al., *Oligonucleotide-modified gold nanoparticles for intracellular gene regulation* Science, 2006. **312**: p. 1027-1030.

14. Hutter, E. and J.H. Fendler, *Exploitation of localized surface plasmon resonance.* Advanced Materials, 2004. **16**: p. 1685-1706.

15. Zheng, Y.B., et al., *Systematic investigation of localized surface plasmon resonance of long-range ordered Au nanodisk arrays.* Journal of Applied Physics, 2008. **103**: p. 014308.

16. Kuncicky, D.M., B.G. Prevo, and O.D. Velev, *Controlled assembly of SERS substrates templated by colloidal crystal films.* Journal of Materials Chemistry, 2006. **16**: p. 1207-1211.

17. Haes, A.J., et al., *Nanoscale optical biosensor: short range distance dependence of the localized surface plasmon resonance of noble metal nanoparticles.* Journal of Physical Chemistry B, 2004. **108**: p. 109.

18. Yonzon, C.R., et al., *A comparative analysis of localized and propagating surface plasmon resonance sensors: the binding of Concanavalin A to a monosaccharide functionalized self-assembled monolayer.* Journal of the American Chemical Society, 2004. **126**: p. 12669.

19. Murray, W.A., J.R. Suckling, and W.L. Barnes, *Overlayers on silver nanotriangles: field confinement and spectral position of localized surface plasmon resonances.* Nano Letters, 2006. **6**: p. 1772-1777.

20. Sun, Y.G. and Y.N. Xia, *Shape-controlled synthesis of gold and silver nanoparticles.* Science, 2002. **298**: p. 2176-2179.

21. Wang, H., et al., *Nanorice: a hybrid plasmonic nanostructure* Nano Letters, 2006. **6**: p. 827-832.

22. Wang, H., et al., *Plasmonic nanostructures: artificial molecules* Accounts of Chemical Research, 2007. **40**: p. 53-62.

23. Yonzon, C.R., et al., *Towards advanced chemical and biological nanosensors - an overview.* Talanta, 2005. **67**: p. 438-448.

24. Halas, N., *Plasmon-based nanoparticle probes for multifunctional diagnostics and therapeutics.* MRS Bulletin, 2005. **30**(Synthesis and plasmonic properties of nanostructures): p. 362.

25. Murphy, C.J., et al., *Anisotropic metal nanoparticles: synthesis, assembly, and optical applications.* MRS Bulletin, 2005. **30**: p. 13857 -13870.

26. Wiley, B., et al., *Shape-controlled synthesis of silver and gold nanostructures.* MRS Bulletin, 2005. **30**: p. 356-361.

27. Xia, Y.N. and N.J. Halas, *Shape-controlled synthesis and surface plasmonic properties of metallic nanostructures.* MRS Bulletin, 2005. **30**: p. 338-348.

28. Krasavin, A.V. and N.I. Zheludev, *Active plasmonics: Controlling signals in Au/Ga waveguide using nanoscale structural transformations.* Applied Physics Letters, 2004. **84**: p. 1416-1418.

29. Soares, B.F., et al., *Polymorphic nanoparticles as all-optical memory elements.* Optics Express, 2006. **14**: p. 10652-10656.

30. Dai, H., *Nanotube growth and characterization.* Carbon Nanotubes, 2001. **80**: p. 29-53.

31. Kneipp, K., et al., *Surface-enhanced and normal Stokes and anti-Stokes Raman spectroscopy of single-walled carbon nanotubes.* Physical Review Letters, 2000. **84**: p. 3470-3473.

32. Michaels, A.M., J. Jiang, and L. Brus, *Ag nanocrystal junctions as the site for surface-enhanced Raman scattering of single rhodamine 6G molecules.* Journal of Physical Chemistry B, 2000. **104**: p. 11965.

33. Moskovits, M., *Surface-enhanced Raman spectroscopy: a brief retrospective.* Journal of Raman Spectroscopy, 2005. **36**: p. 485-496.

34. Le Ru, E.C., et al., *Surface enhanced Raman scattering enhancement factors: a comprehensive study.* Journal of Physical Chemistry B, 2006. **110**: p. 1944-1948.

35. Schadler, L.S., S.C. Giannaris, and P.M. Ajayan, *Load transfer in carbon nanotube epoxy composites.* Applied Physics Letters, 1998. **73**: p. 3842-3844.

36. Shalaev, V.M., et al., *Optical properties of self-affine thin films.* Physical Review B, 1996. **54**: p. 8235-8242.

37. Chan, G.H., et al., *Plasmonic properties of copper nanoparticles fabricated by nanosphere lithography.* Nano Letters, 2007. **7**: p. 1947-1952.

38. Malynych, S. and G. Chumanov, *Light-induced coherent interactions between silver nanoparticles in two-dimensional arrays.* Journal of the American Chemical Society, 2003. **125**: p. 2896-2898.

39. Herrmann, J., et al., *Nanoparticle films as sensitive strain gauges.* Applied Physics Letters, 2007. **91**: p. 183105.

40. Tao, A., P. Sinsermsuksakul, and P. Yang, *Tunable plasmonic lattices of silver nanocrystals.* Nature Nanotechnology, 2007. **2**: p. 435-440.

41. Yan, X., et al., *Fabrication of non-close-packed arrays of colloidal spheres by soft lithography.* Journal of the American Chemical Society, 2005. **127**: p. 7688-7689.